Improved Dehydrogenation Properties of Calcium Borohydride Combined with Alkaline-Earth Metal Amides

ARTICLE *in* THE JOURNAL OF PHYSICAL CHEMISTRY C · AUGUST 2011

Impact Factor: 4.77 · DOI: 10.1021/jp2052695

7 AUTHORS, INCLUDING:

Hailiang Chu
Guilin University of Electronic Technology
67 PUBLICATIONS **854** CITATIONS
SEE PROFILE

Yao Zhang
Southeast University (China)
65 PUBLICATIONS **951** CITATIONS
SEE PROFILE

Jianping Guo
Peking University People's Hospital
35 PUBLICATIONS **398** CITATIONS
SEE PROFILE

THE JOURNAL OF PHYSICAL CHEMISTRY C

ARTICLE

pubs.acs.org/JPCC

Improved Dehydrogenation Properties of Calcium Borohydride Combined with Alkaline-Earth Metal Amides

Hailiang Chu, Guotao Wu, Yao Zhang,* Zhitao Xiong,* Jianping Guo, Teng He, and Ping Chen

Dalian Institute of Chemical Physics, Chinese Academy of Sciences, 457 Zhongshan Road, Dalian, PR China 116023

Supporting Information

ABSTRACT: Promotion of dehydrogenation based on the interaction of $[BH_4]^-$ and $[NH_2]^-$ sources has been demonstrated to be one of the most effective approaches in developing an advanced borohydride/amide hydrogen storage combined system. The $Ca(BH_4)_2$−$2Mg(NH_2)_2$ and $Ca(BH_4)_2$−$2Ca(NH_2)_2$ composites are thereby synthesized in the present work. It is found that the binary combined systems exhibit an onset dehydrogenation temperature of ∼220 °C, which is ∼100 °C lower than that of pristine $Ca(BH_4)_2$. The hydrogen release measurements for $Ca(BH_4)_2$−$2Mg(NH_2)_2$ and $Ca(BH_4)_2$−$2Ca(NH_2)_2$ samples below 480 °C show desorption amounts of 8.3 and 6.8 wt % hydrogen, respectively. The dehydrogenation of both samples is accompanied by an ammonia emission of <1.4 mol %. The characterizations such as X-ray diffraction and nuclear magnetic resonance on the postdehydrogenated samples indicate that the dehydrogenation reactions are in the pathways of $Ca(BH_4)_2 + 2\,Mg(NH_2)_2 \rightarrow 1/3\,[Ca_3Mg_6(BN_2)_6] + 8\,H_2$ and $Ca(BH_4)_2 + 2\,Ca(NH_2)_2 \rightarrow 1/3\,Ca_9(BN_2)_6 + 8\,H_2$, respectively. Compared with pristine $Ca(BH_4)_2$ sample, both possess lower activation energy for dehydrogenation. Further investigation reveals that the interaction of B−H and N−H may be one of main driving forces for dehydrogenation of borohydride/amide combined system.

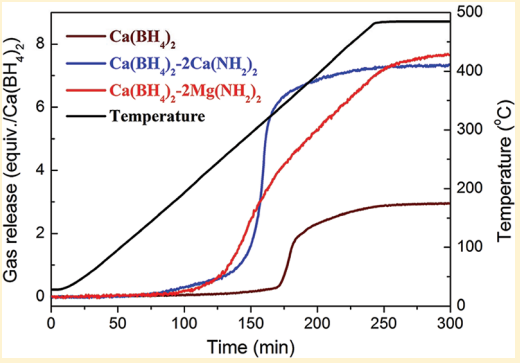

1. INTRODUCTION

The increasing demand for energy, in association with the environmental problems resulting from the use of fossil fuels, is driving the whole society toward using renewable energy. Hydrogen is widely regarded as an environmentally friendly and alternative energy carrier. Hydrogen storage is one of the key technologies for the hydrogen fuel cell vehicles, whereas it is one of the major obstacles to the widespread use of hydrogen as an energy carrier.[1] The year 2015 system targets set by the U.S. Department of Energy are 0.055 kg H_2/kg system and 0.040 kg H_2/L system for on-board hydrogen storage systems.[2] Tremendous efforts has been focused on complex hydrides, especially metal borohydrides,[3−10] which possess large hydrogen capacity and promisingly meet the practical requirements. $LiBH_4$, with a gravimetric density of 18.3%, is one of the most attractive borohydrides.[11−14] However, its major dehydrogenation temperature starting from ca. 380 °C is too high to be practically used. More recently, $Mg(BH_4)_2$ and $Ca(BH_4)_2$ have been known as potential candidates for hydrogen storage. They have more favorable thermodynamic properties than $LiBH_4$[15] while maintaining high hydrogen capacity (14.9 and 11.4 wt %, respectively). It was observed that hydrogen release from $Mg(BH_4)_2$ starts at ∼230 °C in several endothermic steps, and the total amount of 14.4% hydrogen is achieved at ca. 530 °C.[16] $Ca(BH_4)_2$ desorbs 9.0 wt % hydrogen at a temperature as high as 500 °C, and CaH_2 is the only crystalline phase in the solid residue. Additives of fluorides such as Ti or Nb species were introduced to $Ca(BH_4)_2$ to improve the reversibility for hydrogen storage, but their catalytic effect in dehydrogenation is not pronounced.[17−19] Therefore, it is of practical importance to improve the dehydrogenation/rehydrogenation of metal borohydrides.

In 2002, Chen et al. found that Li_3N was an effective hydrogen storage material,[20] which can reversibly store 10.4 wt % hydrogen with larger enthalpy change through the following reaction: $Li_3N + 2H_2 \leftrightarrow Li_2NH + LiH + H_2 \leftrightarrow LiNH_2 + 2LiH$. Recent efforts have focused on the development of many related systems such as Li−Mg−N−H,[21,22] Li−Ca−N−H,[23,24] and Mg−Na−N−H,[25] which have been performed in an effort to improve the dehydrogenation/rehydrogenation behavior of the Li−N−H system. One of the reaction mechanisms was proposed as the dehydrogenation reaction proceeded via coupling solid phase reactions between the amide and the hydride based on the reaction of $H^+ + H^- \rightarrow H_2$ (ΔH = 17.37 eV).[26] Although considerable work has been done on structural identification and kinetic improvement in the metal borohydride for hydrogen storage, it is further hypothesized that the $[BH_4]^-/[NH_2]^-$ system would also have favorable dehydrogenation properties due to the substitution of the $[BH_4]^-$ anion for the bonded H^- in metal hydrides based on a comparison between the metal−N−H

Received: June 5, 2011
Revised: July 20, 2011
Published: July 20, 2011

and metal−B−N−H systems.[20,27] For example, $LiBH_4$−$LiNH_2$,[27,28] $LiBH_4$−$Mg(NH_2)_2$,[29] $Mg(BH_4)_2$−$LiNH_2$,[30] and $Ca(BH_4)_2$−$LiNH_2$[31] systems have been investigated, and the dehydrogenation temperatures of these composites are distinctly lower than those of corresponding metal borohydrides. The chemical interaction between the $[BH_4]^-$ and $[NH_2]^-$ ligands of the composite would facilitate the dehydrogenation and trap N more effectively to reduce the emission of NH_3 from metal amides. In other words, on the basis of the formation of B−N bonds, the combination of $[BH_4]^-$ and $[NH_2]^-$ would proceed adequately because of the short-range effect, and hence it would facilitate the hydrogen release.

In this study, $Ca(BH_4)_2$−$2Mg(NH_2)_2$ and $Ca(BH_4)_2$−$2Ca(NH_2)_2$ composites were prepared by ball milling method. The dehydrogenation performances were studied by temperature-programmed desorption (TPD) and synchronal mass spectroscopy (MS). The product phases and reaction pathways of these samples were characterized by X-ray diffraction (XRD), Fourier transform infrared (FTIR) spectroscopy, and nuclear magnetic resonance (NMR). Furthermore, $Ca(BD_4)_2$ was used to clarify the hydrogen liberation mechanisms occurring in borohydride/amide systems.

2. EXPERIMENTAL SECTION

The starting materials $Ca(BH_4)_2$, $Ca(NH_2)_2$, and $Mg(NH_2)_2$ used in this study were synthesized in our laboratory. The synthetic procedures follow our previous work.[32−34] $Ca(BD_4)_2$ was prepared using $NaBD_4$ instead of $NaBH_4$ under the same condition as $Ca(BH_4)_2$. The subsequent powder XRD (Figure S1 in Supporting Information), FTIR, Raman spectroscopy, and TPD combined with mass spectrometer (TPD−MS) measurements of as-prepared starting materials revealed the synthesis of target samples.

About 1.0 g mixtures of $Ca(BH_4)_2$−$2Mg(NH_2)_2$ and $Ca(BH_4)_2$−$2Ca(NH_2)_2$ were ball-milled using a Retsch PM400 planetary ball mill at 200 rpm for 5 h under an argon atmosphere. The mass ratio of the sample to the steel balls was ∼1:50. All experiments were performed in an argon-filled MBRAUN glovebox with the O_2 and H_2O levels below 1 ppm.

XRD measurements were conducted upon PANalytical X'pert diffractometer to identify the crystalline phase of composites, $Ca(BH_4)_2$, $Ca(NH_2)_2$, and $Mg(NH_2)_2$. The ball-milled $Ca(BH_4)_2$−$2Mg(NH_2)_2$ and $Ca(BH_4)_2$−$2Ca(NH_2)_2$ samples before and after dehydrogenation were characterized through FTIR (Varian 3000) by DRIFT mode. Solid-state ^{11}B magic-angle spinning nuclear magnetic resonance (MAS NMR) experiments were carried out at room temperature on a Bruker AVANCE 500 MHz NMR spectrometer (11.7 T). All of those solid samples were spun at 10 kHz with the use of 4 mm ZrO_2 rotors filled up in a purified argon atmosphere glovebox. The NMR shifts are reported in parts per million (ppm), externally referenced to BF_3OEt_2 at 0 ppm for ^{11}B nuclei.

Hydrogen release measurements were performed on a homemade TPD combined with mass spectrometer (MS, Hiden HPR-20) and a Netzch STA 449C TG/DSC unit. Purified argon was employed as a carrier gas in TPD−MS and TG measurements, in which temperature was raised at a ramping rate of 2 °C/min from 30 to 500 °C. Volumetric release measurements were performed on a Sievert's apparatus. The reactor was heated from room temperature to 480 °C at a heating rate of 2 °C/min or held at 270, 290, and 310 °C for isothermal release. Quantitative measurements of NH_3 concentration in gaseous products

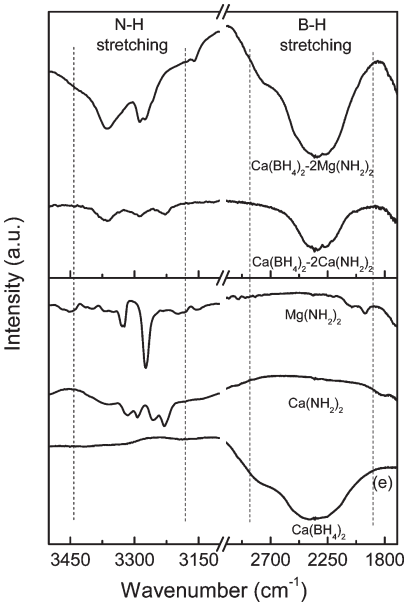

Figure 1. FTIR spectra of ball-milled samples of $Ca(BH_4)_2$−$2Mg(NH_2)_2$ and $Ca(BH_4)_2$−$2Ca(NH_2)_2$. For comparison, FTIR spectra of $Mg(NH_2)_2$, $Ca(NH_2)_2$, and $Ca(BH_4)_2$ are also shown.

obtained from volumetric release measurements were implemented on a thermoconductivity meter (Thermo Scientific, Orion 3-Star) with an accuracy of 0.1 μs/cm, where the outlet gas was introduced to a dilute H_2SO_4 solution (0.6 mmol/L) whose ion conductivity was monitored with the progression of dehydrogenation. It should be noted that the ionic conductivity of the solution will decrease if NH_3 is released from the sample and absorbed by the acid solution. Details of the operation procedure have been described in our previous report.[32]

3. RESULTS AND DISCUSSION

After ball-milling the mixture of $Ca(BH_4)_2$ and $Mg(NH_2)_2$ or $Ca(NH_2)_2$ in a molar ratio of 1:2 for 5 h, the diffraction peaks of starting materials almost disappeared (see Figure S2 in Supporting Information). It indicates the refinement of the crystallite size, the amorphization of post-milled samples, or both. The FTIR result shown in Figure 1 indicates that the characteristic peaks of the N−H bond for $Ca(BH_4)_2$−$2Mg(NH_2)_2$ sample are observed at 3288 and 3364 cm^{-1}, which are completely different from those of pristine $Mg(NH_2)_2$ with two characteristic peaks at 3273 and 3324 cm^{-1}.[35] As for the $Ca(BH_4)_2$−$2Ca(NH_2)_2$ sample, three peaks of the N−H bond in FTIR result shown in Figure 1 are observed at 3228, 3289, and 3372 cm^{-1}, which are also different from those of pristine $Ca(NH_2)_2$ with four characteristic peaks at 3231, 3256, 3292, and 3316 cm^{-1}.[34] Furthermore, a broadened peak related to B−H band was narrowed for $Ca(BH_4)_2$−$2Mg(NH_2)_2$ and $Ca(BH_4)_2$−$2Ca(NH_2)_2$ in comparison with pristine $Ca(BH_4)_2$, even though no hydrogen or ammonia was released from the mixture during ball-milling treatment. Because FTIR results cannot tell the detailed differences of B−H bond for ball-milled samples, ^{11}B MAS NMR spectra were performed on $Ca(BH_4)_2$−$2Mg(NH_2)_2$, $Ca(BH_4)_2$−$2Ca(NH_2)_2$, and pristine $Ca(BH_4)_2$, which are shown in Figure 2. The pristine $Ca(BH_4)_2$ has two resonances at −31.4 and −33.4 ppm assignable to α- and β-phase $Ca(BH_4)_2$,[36] respectively. A single boron species resonating at −34.3 and −35.0 ppm was

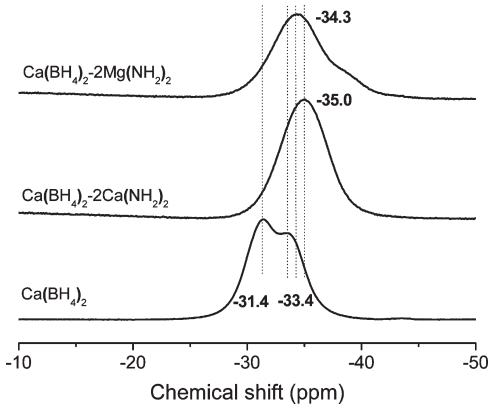

Figure 2. ^{11}B MAS NMR spectra of $Ca(BH_4)_2-2Mg(NH_2)_2$, $Ca(BH_4)_2-2Ca(NH_2)_2$, and pristine $Ca(BH_4)_2$.

observed for $Ca(BH_4)_2-2Mg(NH_2)_2$ and $Ca(BH_4)_2-2Ca(NH_2)_2$ (shown in Figure 2), which has some downfield shift compared with that of pristine $Ca(BH_4)_2$. This suggests that ball-milled $Ca(BH_4)_2-2Mg(NH_2)_2$ and $Ca(BH_4)_2-2Ca(NH_2)_2$ samples are not simply physical mixtures but rather the interacted products between calcium borohydride and alkaline-earth metal amides. On the basis of the primary knowledge, it could be concluded that the combination of $[BH_4]^-$ and $[NH_2]^-$ should taken place during the ball-milling process. A similar interaction between amide and borohydride was reported on $LiBH_4/LiNH_2$,[37] $NaBH_4/NaNH_2$,[38] and $Ca(BH_4)_2/LiNH_2$[32] systems with the formation of new complex hydrides. In this case, however, XRD patterns of these two postmilled samples of $Ca(BH_4)_2-2Mg(NH_2)_2$ and $Ca(BH_4)_2-2Ca(NH_2)_2$ with the high quality were not obtained, even though the postmilled samples were heated to 200 °C for 50 h.

Figures 3 and 4 show TPD−MS, TG, and volumetric release results for ball-milled $Ca(BH_4)_2-2Mg(NH_2)_2$ and $Ca(BH_4)_2-2Ca(NH_2)_2$ samples. The results belonging to starting material $Ca(BH_4)_2$ are also exhibited in the same Figures for comparison. Only one distinct peak of hydrogen evolution can be observed at 360 °C in the MS curve of pristine $Ca(BH_4)_2$, without any detectable diborane and ammonia signal in the MS tracks within the temperature range (20−500 °C). The total desorption capacity up to 480 °C is 3 equiv or 8.6 wt % hydrogen (Figure 4).

In the case of borohydride/amide combined samples, the onset dehydrogenation temperatures were dramatically decreased to 220 °C with one main distinct hydrogen release event. Their peak temperatures were observed at 305 and 313 °C for $Ca(BH_4)_2-2Mg(NH_2)_2$ and $Ca(BH_4)_2-2Ca(NH_2)_2$, respectively. A shoulder at ∼330 °C was found along with the main desorption peak for $Ca(BH_4)_2-2Ca(NH_2)_2$. The onset temperatures of both combined samples are lower than that of pristine $Ca(BH_4)_2$ (∼ 360 °C), indicating significant improvement in the dehydrogenation properties. However, MS analysis in Figure 3 shows that a small quantity of NH_3 release appears from 50 to 300 °C for $Ca(BH_4)_2-2Ca(NH_2)_2$ and from 200 to 300 °C for $Ca(BH_4)_2-2Mg(NH_2)_2$, and no detectable diborane is observed during the hydrogen desorption process, with the total weight loss of 10.8 and 9.4 wt % from TG results. Compared with the pure $Ca(NH_2)_2$ and $Mg(NH_2)_2$ (Figure S3 in Supporting Information), the NH_3 release temperatures for the $Ca(BH_4)_2-2Ca(NH_2)_2$ and $Ca(BH_4)_2-2Mg(NH_2)_2$ samples were decreased significantly. The similar ammonia evolution was observed on $Mg(BH_4)_2/LiNH_2$[30] and

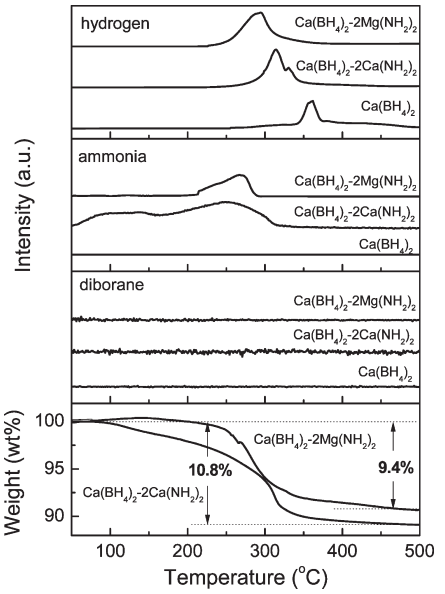

Figure 3. TPD−MS and TG results of ball-milled samples of $Ca(BH_4)_2-2Mg(NH_2)_2$ and $Ca(BH_4)_2-2Ca(NH_2)_2$. For comparison, TPD−MS of pristine $Ca(BH_4)_2$ is also shown.

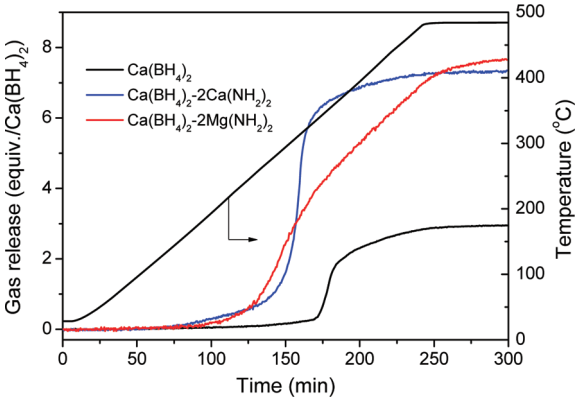

Figure 4. Volumetric release measurements of $Ca(BH_4)_2-2Mg(NH_2)_2$ and $Ca(BH_4)_2-2Ca(NH_2)_2$ samples. For comparison, volumetric release of pristine $Ca(BH_4)_2$ is also shown.

$Ca(BH_4)_2/LiNH_2$[31] combined systems. It means that because of the interaction of $[BH_4]^-$ and $[NH_2]^-$ between borohydride and amide, metal-N bonds may be weakened, causing ammonia release at a lower temperature.

Clearly shown in Figure 4, the dehydrogenation temperature of combined systems is much lower than that of pristine $Ca(BH_4)_2$. In general, sample $Ca(BH_4)_2-2Ca(NH_2)_2$ has a faster dehydrogenation rate than that of $Ca(BH_4)_2-2Mg(NH_2)_2$, especially at higher temperature, from the slope of dehydrogenation curve. Combined with volumetric release and TG results, the capacities of hydrogen desorption, and the amounts of ammonia evolution were calculated and summarized in Table 1. The amounts of ammonia determined by electroconductivity are also shown in Table 1. For the $Ca(BH_4)_2-2Mg(NH_2)_2$ sample, an apparent one-step decomposition was also observed (Figure 3), with the total gas release capacity of 7.6 equiv per $Ca(BH_4)_2$ up to 480 °C (Figure 4). The quantitative measurement indicated that there is only 1.4 mol % of ammonia generated in the evolved gas when

dx.doi.org/10.1021/jp2052695 |J. Phys. Chem. C 2011, 115, 18035–18041

Table 1. Summary of H_2 and NH_3 Content in the Desorbed Gas of Ball-Milled $Ca(BH_4)_2-2Mg(NH_2)_2$ and $Ca(BH_4)_2-2Ca(NH_2)_2$ Samples Heated to 480 °C

samples	weight loss from TG (wt %)	volumetric release (equiv per $Ca(BH_4)_2$)	cal. NH_3 content in desorbed gas (mol %)[a]	exp. NH_3 content in desorbed gas (mol %)	exp. H_2 content in desorbed gas (mol %)[b]	H_2 content (wt %)[c]
$Ca(BH_4)_2-2Ca(NH_2)_2$	10.8	7.3	7.6	1.3	98.7	6.8
$Ca(BH_4)_2-2Mg(NH_2)_2$	9.4	7.6	1.7	1.4	98.6	8.3

[a] Calculated values based on volumetric release and TG results. [b] Subtracting the amount of ammonia obtained from electroconductivity. [c] (Desorbed hydrogen)/(initial weight of calcium borohydride and alkaline-earth metal amide in a molar ratio of 1:2).

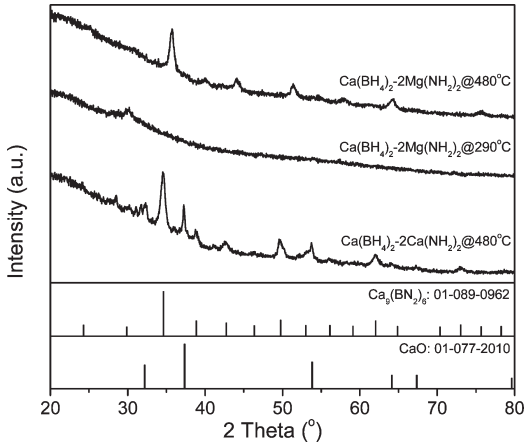

Figure 5. XRD patterns for postdehydrogenated $Ca(BH_4)_2-2Ca(NH_2)_2$ at 480 °C, $Ca(BH_4)_2-2Mg(NH_2)_2$ at 290 °C, and $Ca(BH_4)_2-2Mg(NH_2)_2$ at 480 °C after volumetric release measurements.

heated to 480 °C. That is to say, as high as 7.5 equiv of hydrogen (or 8.3 wt %) can be desorbed from the $Ca(BH_4)_2-2Mg(NH_2)_2$ sample, accompanied by 0.1 equiv per $Ca(BH_4)_2$ of ammonia emission. In the case of $Ca(BH_4)_2-2Ca(NH_2)_2$ sample, there is only 0.09 equiv ammonia in all evolved gas of 7.3 equiv per $Ca(BH_4)_2$, indicating that the hydrogen desorption capacity is 6.8 wt %. It is noted that the amount of ammonia determined by experimental electroconductivity measurement is much lower than the calculated value based on volumetric release and TG results (Table 1). That means that the sample desorbs more ammonia in open system (TG and TPD measurements) than in closed reactor (volumetric release measurement). This point was clarified in our previous study.[9] Ammonia can react with metal borohydrides to produce hydrogen in closed vessel because of equilibrium NH_3 vapor pressure control, whereas under dynamic flow mode (i.e., TG) ammonia has been immediately detached from sample by the carrier gas (argon). The aforementioned TG−MS and volumetric release results clearly indicate that the dehydrogenation of $Ca(BH_4)_2$ can be improved significantly when it is combined with alkaline-earth metal amides, although there is trace ammonia emission during hydrogen desorption process.

To clarify the reactions occurring in dehydrogenation process, we carried out XRD, FTIR, and NMR measurements on the postdehydrogenated samples. Figure 5 shows the XRD patterns for $Ca(BH_4)_2-2Ca(NH_2)_2$, and $Ca(BH_4)_2-2Mg(NH_2)_2$ samples after dehydrogenation up to 480 °C. For $Ca(BH_4)_2-2Ca(NH_2)_2$ sample, the XRD pattern shows that $Ca_9(BN_2)_6$ rather than CaH_2 is observed except for some CaO after dehydrogenation at 480 °C. As shown in Figure S4 in the Supporting Information, NMR result indicates that a broad line shape with two peaks at 7.2 and 19.5 ppm was detectable for postdehydrogenated $Ca(BH_4)_2-2Ca(NH_2)_2$, which is due to the second-order quadrupolar interaction. A similar line shape was observed in the study of $Ca_3(BN_2^{3-})_2$.[39] Taking the hydrogen desorption capacity into consideration, the dehydrogenation reactions can be expressed

$$Ca(BH_4)_2 + 2Ca(NH_2)_2 \rightarrow 1/3Ca_9(BN_2)_6 + 8H_2(7.5\ \text{wt}\ \%\ H_2) \quad (1)$$

In the case of $Ca(BH_4)_2-2Mg(NH_2)_2$ sample, when heated to 480 °C, the detectable chemical shift of −33.2 ppm assigned to residual BH_4^- group was observed in NMR spectrum (Figure S4 in Supporting Information). However, there is no BH_4^- signal in NMR spectrum for postdehydrogenated $Ca(BH_4)_2-2Ca(NH_2)_2$, which indicates higher kinetic barriers for $Ca(BH_4)_2-2Mg(NH_2)_2$ dehydrogenation to overcome than that of $Ca(BH_4)_2-2Ca(NH_2)_2$. The XRD result shows a set of peaks at 2θ degrees of 35.7, 40.0, 44.2, 51.2, 58.1, and 64.3°. Compared with the diffraction peaks of $Ca_9(BN_2)_6$, these peaks have shifted to higher 2θ angle. We ascribed these peaks to $[Ca_3Mg_6(BN_2)_6]$ with lattice parameter of a = 7.1057 Å (space group: $Im3m$) according to the following dehydrogenation reaction

$$Ca(BH_4)_2 + 2Mg(NH_2)_2 \rightarrow 1/3[Ca_3Mg_6(BN_2)_6] + 8H_2(8.8\ \text{wt}\ \%\ H_2) \quad (2)$$

Moreover, the ^{11}B MAS NMR spectrum presents a similar line shape of postdehydrogenated $Ca(BH_4)_2-2Mg(NH_2)_2$ as $Ca(BH_4)_2-2Ca(NH_2)_2$ except for residual BH_4^- at −33.2 ppm (Figure S4 in Supporting Information), indicating similar chemical environment of boron in the solid residue. The lattice parameter of $[Ca_3Mg_6(BN_2)_6]$ is smaller than that of $Ca_9(BN_2)_6$ (7.3224 Å), which is related to the fact that the radius of Mg^{2+} (0.66 Å) is smaller than that of Ca^{2+} (0.99 Å). It should be noted that volumetric release results of 8.3 and 6.8 wt % are lower than the theoretical values of 8.8 and 7.5 wt % for $Ca(BH_4)_2-2Mg(NH_2)_2$ and $Ca(BH_4)_2-2Ca(NH_2)_2$, respectively. This fact may be resulting from some factors: (1) the ammonia evolution, (2) the formation of CaO, and (3) BH_4^- left in the postdehydrogenated $Ca(BH_4)_2-2Mg(NH_2)_2$. Our preliminary attempt of rehydrogenating the postdehydrogenated powder under a H_2 pressure of 50 bar in the temperature range of 20−300 °C was unsuccessful.

To shine a light on the thermodynamic and kinetic properties of dehydrogenation of these two combined samples, $Ca(BH_4)_2-2Mg(NH_2)_2$ and $Ca(BH_4)_2-2Ca(NH_2)_2$ underwent volumetric release at 270, 290, and 310 °C. For $Ca(BH_4)_2-2Ca(NH_2)_2$ sample, as shown in Figure 6, ca. 2.5, 5.0, and 6.0 wt % hydrogen can be released in about 480, 500, and 200 min at 270, 290, and 310 °C, respectively. In the case of $Ca(BH_4)_2-2Mg(NH_2)_2$ sample, it can release 6.1, 6.5, and 7.0 wt % hydrogen in about 740, 850, and 370 min at the same temperatures. In other words,

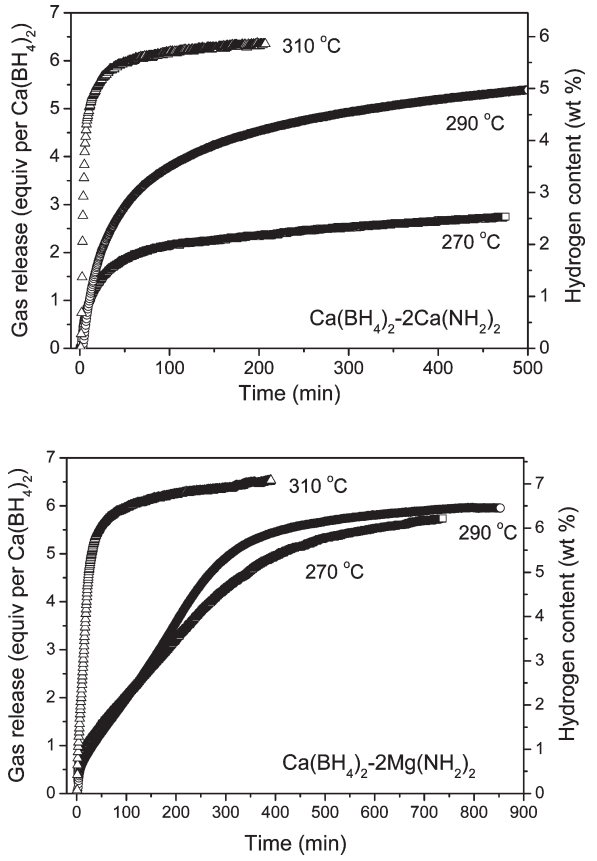

Figure 6. Isothermal dehydrogenation kinetics of ball-milled $Ca(BH_4)_2-2Ca(NH_2)_2$ and $Ca(BH_4)_2-2Mg(NH_2)_2$ samples under initially mechanical vacuum at different temperatures. Hydrogen desorption capacity with the unit of wt % in right *Y* axis is calculated excluding ammonia.

some hydrogen remained in these samples, which is confirmed from the N−H and B−H signals in ^{11}B MAS NMR (Figure S4 in Supporting Information) and FTIR (Figure S5 in Supporting Information) spectra of postdehydrogenated $Ca(BH_4)_2-2Mg(NH_2)_2$ sample at 290 °C. XRD characterization shows that no structural information can be obtained from the postdehydrogenated $Ca(BH_4)_2-2Mg(NH_2)_2$ sample (Figure 5), because of the amorphous phases in nature. It is also reasonable to assign the slower dehydrogenation at lower temperature to the presence of kinetic barriers rather than thermodynamic constraint, where catalytic modification is needed to optimize further calcium borohydride/alkaline-earth metal amide for hydrogen storage.

To obtain the distinctly enhanced kinetics of $Ca(BH_4)_2-2Ca(NH_2)_2$ and $Ca(BH_4)_2-2Mg(NH_2)_2$, we adopted Kissinger's method in determining the activation energy

$$\ln(\beta/T_m^2) = -E_a/R + \ln(AR/E_a) \quad (3)$$

Here T_m is the temperature at which the maximum reaction rate peaks, β is the heating rate, E_a is the activation energy, A is the pre-exponential factor, and R is the gas constant. The maximum reaction-rate temperatures at various heating rates were collected by means of TPD measurements. Figure 7 summarized the TPD profiles of hydrogen desorption from the $Ca(BH_4)_2-2Ca(NH_2)_2$ and $Ca(BH_4)_2-2Mg(NH_2)_2$ at different ramping rates. We observed that the peak temperatures shifted monotonically to higher values when the ramping rate increased from 1 to 4 °C/

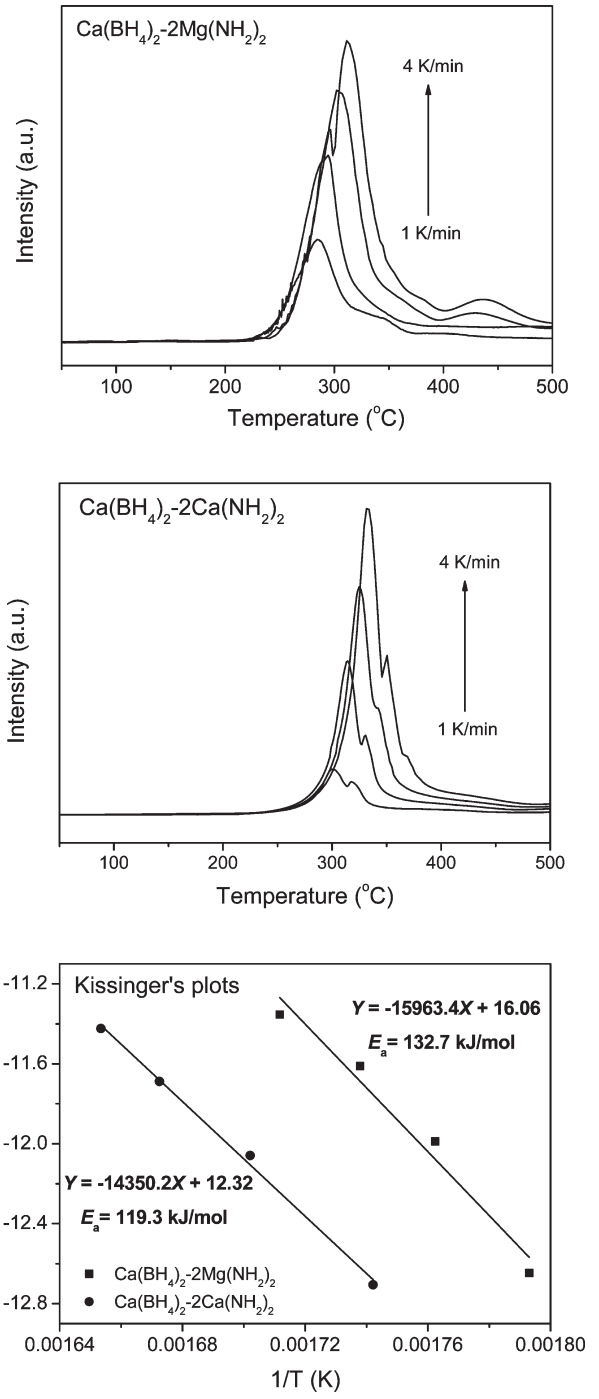

Figure 7. TPD profiles of hydrogen desorption from $Ca(BH_4)_2-2Mg(NH_2)_2$ and $Ca(BH_4)_2-2Ca(NH_2)_2$ at different ramping rates. Kissinger's plots, which give the activation energy of $Ca(BH_4)_2-2Ca(NH_2)_2$ and $Ca(BH_4)_2-2Mg(NH_2)_2$.

min. The dependence of $\ln(\beta/T_m^2)$ to $1/T_m$ is also plotted in Figure 7. The slope and the intercept of the fitted line are used to determine the values of E_a and A, respectively. Once E_a and A are known, the specific rate constant k at given temperature can be determined by the Arrhenius equation

$$k = A\exp(-E_a/RT) \quad (4)$$

Table 2 summarizes E_a, A, and k (at 300 °C) for each sample. As mentioned above, the rate constant k at 300 °C of

dx.doi.org/10.1021/jp2052695 |J. Phys. Chem. C 2011, 115, 18035–18041

Table 2. E_a, A, and k (at 300 °C) Calculated from Kissinger Equation and Arrhenius Equation

	E_a (kJ/mol)	A (min^{-1})	k (min^{-1})
$Ca(BH_4)_2$−$2Ca(NH_2)_2$	119.3	3.2×10^9	4.3×10^{-2}
$Ca(BH_4)_2$−$2Mg(NH_2)_2$	132.7	1.5×10^{10}	1.2×10^{-2}

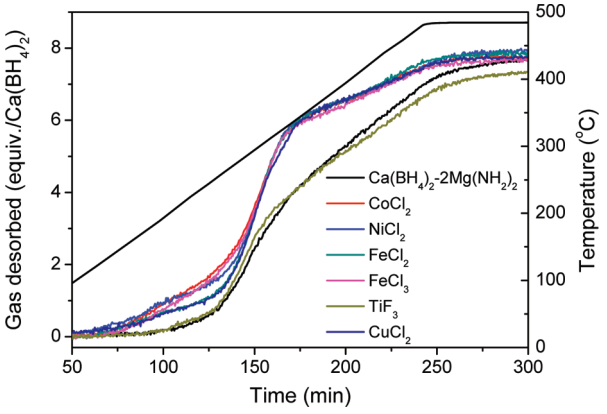

Figure 8. Desorption profiles of sample $Ca(BH_4)_2$−$2Mg(NH_2)_2$ with 10 wt % addition of various additives.

$Ca(BH_4)_2$−$2Ca(NH_2)_2$ is larger than that of $Ca(BH_4)_2$−$2Mg(NH_2)_2$, which agrees with the order of hydrogen release rate determined in volumetric release measurements. The activation energy E_a for hydrogen desorption from the $Ca(BH_4)_2$−$2Ca(NH_2)_2$ and $Ca(BH_4)_2$−$2Mg(NH_2)_2$ is around 119.3 and 132.7 kJ/mol, respectively. The obtained E_a is lower than that of pristine $Ca(BH_4)_2$ of 225.4 kJ/mol,[40] $Ca(BH_4)_2$−$4LiNH_2$ of 138.6 kJ/mol,[32] suggesting a considerable enhancement in dehydrogenation kinetics of pristine $Ca(BH_4)_2$ after being combined with alkaline-earth metal amides. Because $Ca(BH_4)_2$−$2Mg(NH_2)_2$ sample has higher activation energy (E_a = 132.7 kJ/mol) and slower rate ($k = 1.2 \times 10^{-2}$ min^{-1}) for hydrogen desorption, the effect of additives as shown in Figure 8 is investigated. No matter what the chloride is ($FeCl_2$, $CoCl_2$, $FeCl_3$, $NiCl_2$, $CuCl_2$), all of the samples show significant improvement of the dehydrogenation but with slow dehydrogenation rates during heating. This may be related the fact that metal particles formed from the reduction of metal cations by borohydride have poor crystallinity and are finely dispersed sample, which could lead to a high catalytic efficiency.[41] However, the addition of TiF_3 has no catalytic effect on eith dehydrogenation temperature or rate. Then, the calcium borohydride/alkali-earth metal amide combined system can be regarded as one of the potential candidates for hydrogen storage if the evolution of ammonia during hydrogen desorption will be suppressed and the dehydrogenation temperature will be further decreased.

As mentioned in the Introduction, H in $Ca(NH_2)_2$ is partially positively charged, but in $Ca(BH_4)_2$, it is negatively charged. The redox of $H^{\delta+}$ and $H^{\delta-}$ to H_2 and simultaneously combination of $N^{\delta-}$ and $B^{\delta+}$ is understandable. The shorter H−B···N−H distance between the $[BH_4]^-$ and $[NH_2]^-$ ligands of the composite would facilitate the dehydrogenation. In other words, as a fact of the formation of B−N bonds, the interaction of $[BH_4]^-$ and $[NH_2]^-$ should proceed adequately and facilitate the hydrogen release because of the short-range effect. In this context, HD should be the main gaseous product if $Ca(BD_4)_2$ is used instead of $Ca(BH_4)_2$ in this interaction. To test this idea, we prepared $Ca(BD_4)_2$−$2Ca(NH_2)_2$ sample for TPD measurement. There was no H−D isotopic exchange during the preparation because no N−D and B−H vibrations are observed in FTIR spectrum (Figure S6 in Supporting Information) because of the opposite charges between H and D. To our surprise, the desorbed gas is a mixture of H_2, HD, and D_2 shown in Figure 9. Because HD is one of the main gaseous products, the interaction of B−H in borohydride and N−H in amide should be one of the driving forces for dehydrogenation. The observed distribution of the desorbed gases is actually the result of multiple H−D exchanges among solid transition states, products, and gaseous products, which are strongly influenced by the reaction conditions, such as temperature, gas flow rate, and so on. It is worth mentioning that the H−D exchange during dehydrogenation reaction will bring complications (i.e., isotopic effect) to the attempts in identifying the reaction mechanism by quantitatively measuring the gaseous products, that is, the relative amount of H_2, HD, and D_2.[42,43] Therefore, we suggest that more investigations are needed for the mechanistic understanding.

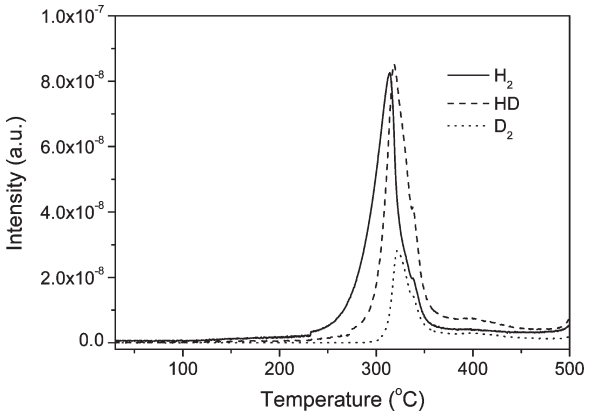

Figure 9. MS signals of H_2, HD, and D_2 detected in TPD measurements over $Ca(BD_4)_2$−$2Ca(NH_2)_2$ sample.

4. CONCLUSIONS

In the present study, the dehydrogenation properties of $Ca(BH_4)_2$ combined with $Mg(NH_2)_2$ or $Ca(NH_2)_2$ were systematically investigated. It has been demonstrated that the calcium borohydride/amide system, releasing hydrogen with onset temperature of 220 °C, shows a significant improvement in the dehydrogenation kinetics and thermodynamics over those of pure $Ca(BH_4)_2$. In the temperature range of 30−500 °C, the $Ca(BH_4)_2$−$2Mg(NH_2)_2$ and $Ca(BH_4)_2$−$2Mg(NH_2)_2$ present a hydrogen desorption capacity of 8.3 and 6.8 wt % in the dehydrogenation pathways of $Ca(BH_4)_2 + 2Mg(NH_2)_2 \rightarrow 1/3[Ca_3Mg_6(BN_2)_6] + 8H_2$ and $Ca(BH_4)_2 + 2Ca(NH_2)_2 \rightarrow 1/3Ca_9(BN_2)_6 + 8H_2$, respectively. Simultaneously, the amount of ammonia emission is <1.4 mol %. The additives of transition-metal chlorides can significantly improve the dehydrogenation of sample $Ca(BH_4)_2$−$2Mg(NH_2)_2$. Furthermore, our isotopic experiments of $Ca(BD_4)_2$−$2Ca(NH_2)_2$ have provided solid evidence of the interaction of B−H and N−H as one of main driving forces for dehydrogenation, which will bring further insight into developing the metal−B−N−H hydrogen storage system.

■ ASSOCIATED CONTENT

Supporting Information. XRD patterns of all starting materials and ball-milled $Ca(BH_4)_2-2Ca(NH_2)_2$ and $Ca(BH_4)_2-2Mg(NH_2)_2$ samples. TG−MS profiles of $Mg(NH_2)_2$ and $Ca(NH_2)_2$. ^{11}B MAS NMR spectra for postdehydrogenated $Ca(BH_4)_2-2Ca(NH_2)_2$ and $Ca(BH_4)_2-2Mg(NH_2)_2$ samples. FTIR spectra of postdehydrogenated $Ca(BH_4)_2-2Mg(NH_2)_2$ at 290 °C and ball-milled $Ca(BD_4)_2$-$2Ca(NH_2)_2$. This material is available free of charge via the Internet at http://pubs.acs.org.

■ AUTHOR INFORMATION

Corresponding Author

*E-mail: zhangyao@dicp.ac.cn (Y.Z.), xzt@dicp.ac.cn (Z.X.). Tel/Fax: +86 411 84379583.

■ ACKNOWLEDGMENT

We acknowledge the financial support from the Hundred Talents Project of the Chinese Academy of Sciences (no. KGCX2-YW-806), National Natural Science Foundation of China (no. 50901070, 20971120, and 20973162), Science and Technology Plan of Dalian (no. 2009J22DW016), and the Ph.D. Startup Foundation of Liaoning Province (no. 20101113). We are grateful to Ms. Xiaohua Ju for NMR measurements.

■ REFERENCES

(1) Schlapbach, L.; Züttel, A. *Nature* **2001**, *414*, 353–358.

(2) *Hydrogen Fuel Cells and Infrastructure Technologies Program: Multiyear Research Development and Demonstration Plan, Part 3.3*, 2009. U.S. Department of Energy. http://www1.eere.energy.gov/hydrogenandfuelcells/mypp/pdfs/storage.pdf (accessed April 2009).

(3) Züttel, A.; Wenger, P.; Rentsch, S.; Sudan, P.; Mauron, P.; Emmenegger, C. *J. Power Sources* **2003**, *118*, 1–7.

(4) Orimo, S.; Nakamori, Y.; Ohba, N.; Miwa, K.; Aoki, M.; Towata, S.; Züttel, A. *Appl. Phys. Lett.* **2006**, *89*, 021920.

(5) Newhouse, R. J.; Stavilla, V.; Hwang, S. J.; Klebanoff, L. E.; Zhang, J. Z. *J. Phys. Chem. C* **2010**, *114*, 5224–5232.

(6) Pinkerton, F. E.; Meyer, M. S. *J. Alloys Compd.* **2008**, *464*, L1–L4.

(7) Pendolino, F.; Mauron, P.; Borgschulte, A.; Züttel, A. *J. Phys. Chem. C* **2009**, *113*, 17231–17234.

(8) Ronnebro, E.; Majzoub, E. H. *J. Phys. Chem. B* **2007**, *111*, 12045–12047.

(9) Chu, H. L.; Wu, G. T.; Xiong, Z. T.; Guo, J. P.; He, T.; Chen, P. *Chem. Mater.* **2010**, *22*, 6021–6028.

(10) Li, H. W.; Kikuchi, K.; Nakamori, Y.; Ohba, N.; Miwa, K.; Towata, S.; Orimo, S. *Acta Mater.* **2008**, *56*, 1342–1347.

(11) Blanchard, D.; Shi, Q.; Boothroyd, C. B.; Vegge, T. *J. Phys. Chem. C* **2009**, *113*, 14059–14066.

(12) Fang, Z. Z.; Kang, X. D.; Dai, H. B.; Zhang, M. J.; Wang, P.; Cheng, H. M. *Scr. Mater.* **2008**, *58*, 922–925.

(13) Yu, X. B.; Grant, D. M.; Walker, G. S. *J. Phys. Chem. C* **2009**, *113*, 17945–17949.

(14) Züttel, A.; Rentsch, S.; Fischer, P.; Wenger, P.; Sudan, P.; Mauron, P.; Emmenegger, C. *J. Alloys Compd.* **2003**, *356−357*, 515–520.

(15) Nakamori, Y.; Miwa, K.; Ninomiya, A.; Li, H. W.; Ohba, N.; Towata, S.; Züttel, A.; Orimo, S. *Phys. Rev. B* **2006**, *74*, 045126.

(16) Li, H. W.; Kikuchi, K.; Sato, T.; Nakamori, Y.; Ohba, N.; Aoki, M.; Miwa, K.; Towata, S.; Orimo, S. *Mater. Trans.* **2008**, *49*, 2224–2228.

(17) Kim, J. H.; Shim, J. H.; Cho, Y. W. *J. Power Sources* **2008**, *181*, 140–143.

(18) Minella, C. B.; Garroni, S.; Pistidda, C.; Gosalawit-Utke, R.; Barkhordarian, G.; Rongeat, C.; Lindemann, I.; Gutfleisch, O.; Jensen, T. R.; Cerenius, Y.; Christensen, J.; Baro, M. D.; Bormann, R.; Klassen, T.; Dornheim, M. *J. Phys. Chem. C* **2011**, *115*, 2497–2504.

(19) Gosalawit-Utke, R.; Suarez, K.; von Colbe, J. M. B.; Bösenberg, U.; Jensen, T. R.; Cerenius, Y.; Minella, C. B.; Pistidda, C.; Barkhordarian, G.; Schulze, M.; Klassen, T.; Bormann, R.; Dornheim, M. *J. Phys. Chem. C* **2011**, *115*, 3762–3768.

(20) Chen, P.; Xiong, Z. T.; Luo, J. Z.; Lin, J. Y.; Tan, K. L. *Nature* **2002**, *420*, 302–304.

(21) Luo, W. F. *J. Alloys Compd.* **2004**, *381*, 284–287.

(22) Wang, J. H.; Liu, T.; Wu, G. T.; Li, W.; Liu, Y. F.; Araujo, C. M.; Scheicher, R. H.; Blomqvist, A.; Ahuja, R.; Xiong, Z. T.; Yang, P.; Gao, M. X.; Pan, H. G.; Chen, P. *Angew. Chem., Int. Ed.* **2009**, *48*, 5828–5832.

(23) Tokoyoda, K.; Hino, S.; Ichikawa, T.; Okamoto, K.; Fujii, H. *J. Alloys Compd.* **2007**, *439*, 337–341.

(24) Chu, H. L.; Xiong, Z. T.; Wu, G. T.; He, T.; Wu, C. Z.; Chen, P. *Int. J. Hydrogen Energy* **2010**, *35*, 8317–8321.

(25) Xiong, Z. T.; Hu, J. J.; Wu, G. T.; Chen, P. *J. Alloys Compd.* **2005**, *395*, 209–212.

(26) Xiong, Z. T.; Wu, G. T.; Hu, J. J.; Chen, P. *Adv. Mater.* **2004**, *16*, 1522–1525.

(27) Pinkerton, F. E.; Meisner, G. P.; Meyer, M. S.; Balogh, M. P.; Kundrat, M. D. *J. Phys. Chem. B* **2005**, *109*, 6–8.

(28) Noritake, T.; Aoki, M.; Towata, S.; Ninomiya, A.; Nakamori, Y.; Orimo, S. *Appl. Phys. A: Mater. Sci. Process.* **2006**, *83*, 277–279.

(29) Chen, X. Y.; Guo, Y. H.; Yu, X. B. *J. Phys. Chem. C* **2010**, *114*, 17947–17953.

(30) Yu, X. B.; Guo, Y. H.; Sun, D. L.; Yang, Z. X.; Ranjbar, A.; Guo, Z. P.; Liu, H. K.; Dou, S. X. *J. Phys. Chem. C* **2010**, *114*, 4733–4737.

(31) Chu, H. L.; Xiong, Z. T.; Wu, G. T.; Guo, J. P.; He, T.; Chen, P. *Dalton Trans.* **2010**, *39*, 10585–10587.

(32) Chu, H. L.; Xiong, Z. T.; Wu, G. T.; Guo, J. P.; Zheng, X. L.; He, T.; Wu, C. Z.; Chen, P. *Chem. −Asian J.* **2010**, *5*, 1594–1599.

(33) Xiong, Z. T.; Hu, J. J.; Wu, G. T.; Chen, P.; Luo, W. F.; Gross, K.; Wang, J. *J. Alloys Compd.* **2005**, *398*, 235–239.

(34) Xiong, Z. T.; Wu, G. T.; Hu, J. J.; Chen, P. *J. Alloys Compd.* **2007**, *441*, 152–156.

(35) Liu, Y. F.; Hu, J. J.; Wu, G. T.; Chen, P. *J. Phys. Chem. C* **2007**, *111*, 19161–19164.

(36) Reiter, J. W.; Zan, J. A.; Bowman, R. C., Jr.; Hwang, S. J. DOE 2009 Annual Progress Report. http://www.hydrogen.energy.gov/pdfs/review09/stp_38_reiter.pdf (accessed May 20, 2009).

(37) Chater, P. A.; David, W. I. F.; Anderson, P. A. *Chem. Commun.* **2007**, 4770–4772.

(38) Somer, M.; Acar, S.; Koz, C.; Kokal, I.; Höhn, P.; Cardoso-Gil, Raul.; Aydemir, U.; Akselrud, L. *J. Alloys Compd.* **2010**, *491*, 98–105.

(39) Wörle, M.; Altenschildesche, H. M.; Nesper, R. *J. Alloys Compd.* **1998**, *264*, 107–114.

(40) Mao, J. F.; Guo, Z. P.; Poh, C. K.; Ranjbar, A.; Guo, Y. H.; Yu, X. B.; Liu, H. K. *J. Alloys Compd.* **2010**, *500*, 200–205.

(41) Tang, W. S.; Wu, G. T.; Liu, T.; Wee, A. T. S.; Yong, C. K.; Xiong, Z. T.; Hora, A. T. S.; Chen, P. *Dalton Trans.* **2008**, *18*, 2395–2399.

(42) Chen, P.; Luo, J. Z.; Xiong, Z. T.; Lin, J. Y.; Tan, K. L. *J. Phys. Chem. B* **2003**, *107*, 10967–10970.

(43) Isobe, S.; Ichikawa, T.; Hino, S.; Fujii, H. *J. Phys. Chem. B* **2005**, *109*, 14855–14858.